Meteorological Assessment of SRM Exhaust Products' Environmental Impact

A. Nelson Dingle

NASA Grant No. NSG-1243

Final Report

Table of Contents

List of Figures and Tables

I. Introduction

This is the final report of research conducted since 1976 under NASA Grant NSG-1243 under the general title "Rain Scavenging of Solid Rocket Exhaust Clouds". The requirement addressed by the work is that of assessing the environmental impact of Solid Rocket Motor (SRM) exhaust products discharged into the free air stream upon the launching of space vehicles that depend upon SRM boosters to obtain large thrust. These include the Titan series and especially the Space Shuttle.

The exhaust product of greatest concern is HCl gas, of which the Space Shuttle boosters generate and discharge 128,900 kg to the air below 10 km (troposphere). In addition 142,543 kg of H_2O and 174,900 kg of Al_2O_3 are emitted to the troposphere from the SRMs in each Shuttle launch. The Al_2O_3 appears as particles suitable for heterogeneous nucleation of HCl_{aq} (hydrochloric acid) which under frequently occurring atmospheric conditions may form a highly acidic rain capable of damaging property and crops and of impacting upon the health of human and animal populations.

The meteorological assessment of this problem has numerous aspects. The present work has addressed two of these, namely, (a) the cloud processes leading to the formation of acid rain and the concentration of the acid that then reaches the ground, and (b) the atmospheric situations that lead to the production of cloud and rain at and near a launch site, and the prediction of weather conditions that may permit or prohibit a launch operation.

In Section II of this report we present our analysis of the heterogeneous condensation/evaporation of HCl and H_2O under conditions found in Titan III exhaust clouds ("ground cloud") some 90 sec after launch at about 1 km altitude. This provides basic information that should be used in a cloud/rain microphysical model to predict rainfall occurrence and acid concentration.

Section III presents a numerical method for use in generating weather predictions by means of our 3-D Mesoscale Model (Hsu, 1979).

II. The Co-Condensation/Evaporation of HCl and H_2O

The free energy change, ΔF, of a system is a measure of the tendency of that system to progress from one thermodynamic state to another. For the case of condensation/evaporation of i different vapors on wettable particles, the general expression is

$$\Delta F = 4\pi\sigma'(a^2 - r_p^2) - \sum_i (\dot{n}_i \, kT \ln S_i') \qquad (1)$$

where

- σ' is the surface energy per unit area of the droplet surface
- a is the radius of the droplet
- r_p is the radius of the nucleating particle
- $\dot{n}_i$ is the number of i-molecules condensed on the drop
- k is Boltzmann's constant
- T is the absolute temperature of the droplet surface
- S_i' is the saturation ratio of vapor i with respect to a flat surface of bulk solution at the same concentration as the droplet

The present purpose is to explore the application of this basic thermodynamic statement to the case of the co-condensation/evaporation of H_2O and HCl vapors on wettable particles in the open air. For this case, let i = 1 specify H_2O and i = 2 HCl, and let the HCl molefraction, x_2, express the solution concentration. By definition, then, the molality, $M = 55.5\ x_2/(1 - x_2) = 55.5\ f(x_2)$.

The drop radius is

$$a = \left[\frac{3}{4\pi}\ \frac{\dot{n}_1\dot{m}_1}{\rho' n_0}\ (1 + f(x_2)\beta) + r_p^{\,3}\right]^{1/3} \qquad (2)$$

where

$\dot{m}_1$ is the mass of a molecule of H_2O

ρ' is the solution density

n_0 is Avogadro's number

β is M_2/M_1 and M_i is the molecular weight of i.

Empirical expressions are used for the solution surface energy,

$$\sigma' = 75.728 - 0.1535(T-273.16) - 10.575f(x_2) \qquad (3)$$

and the solution density

$$\rho' = 1.0 - 0.72158\ f(x_2) \qquad (4)$$

The saturation ratio for each vapor with respect to a flat surface of the solution is given by

$$S_i' = P_i/P_i^{\,sat}(x_2,T) \qquad (5)$$

where

P_i is the environmental partial pressure of i

and

$P_i^{sat}(x_2,T)$ is the equilibrium vapor pressure of i over a flat surface of solution of concentration x_1 and temperature T.

For T = 288° K, the values of S_1' and S_2' as functions of x_2 are shown in Fig. 1. Note that $S_2' > 1$ only for $x_2 < 8.85 \times 10^{-2}$, whereas $S_1' > 1$ only for $x_2 > 8.15 \times 10^{-2}$, hence at 288° K, the vapors are both supersaturated with respect to the bulk solution only in the narrow HCl molefraction range of $8.15 \times 10^{-2} \leq x_2 \leq 8.85 \times 10^{-2}$.

By means of (2), (3), (4) and (5), ΔF may now be expressed in terms of the six variables P_1, P_2, T, $\dot{n}_i$, r_p, and x_2. For any particular case, the environmental values of P_1, P_2 and T must be specified, thus ΔF may be expressed for such a case in terms of r_p, $\dot{n}_i$ and x_2.

The total number of molecules, $\dot{n}_s$, required to form a monolayer of solution on a particle may be estimated as a function of r_p and x_2 as follows. If the particle and its coating of solution is spherical, then $\dot{n}_s$ is given by

$$\dot{n}_s = \dot{n}_1 + \dot{n}_2 = 4 \left(1 + \frac{r_p}{\dot{r}_s}\right)^2 \qquad (6a)$$

also $$\dot{n}_1 = 4\left(1 + \frac{r_p}{\dot{r}_s}\right)^2 / \left(1 + f(x_2)\right) \qquad (6b)$$

where $\dot{r}_s$ is the mean molecular radius of a "molecule" of solution,

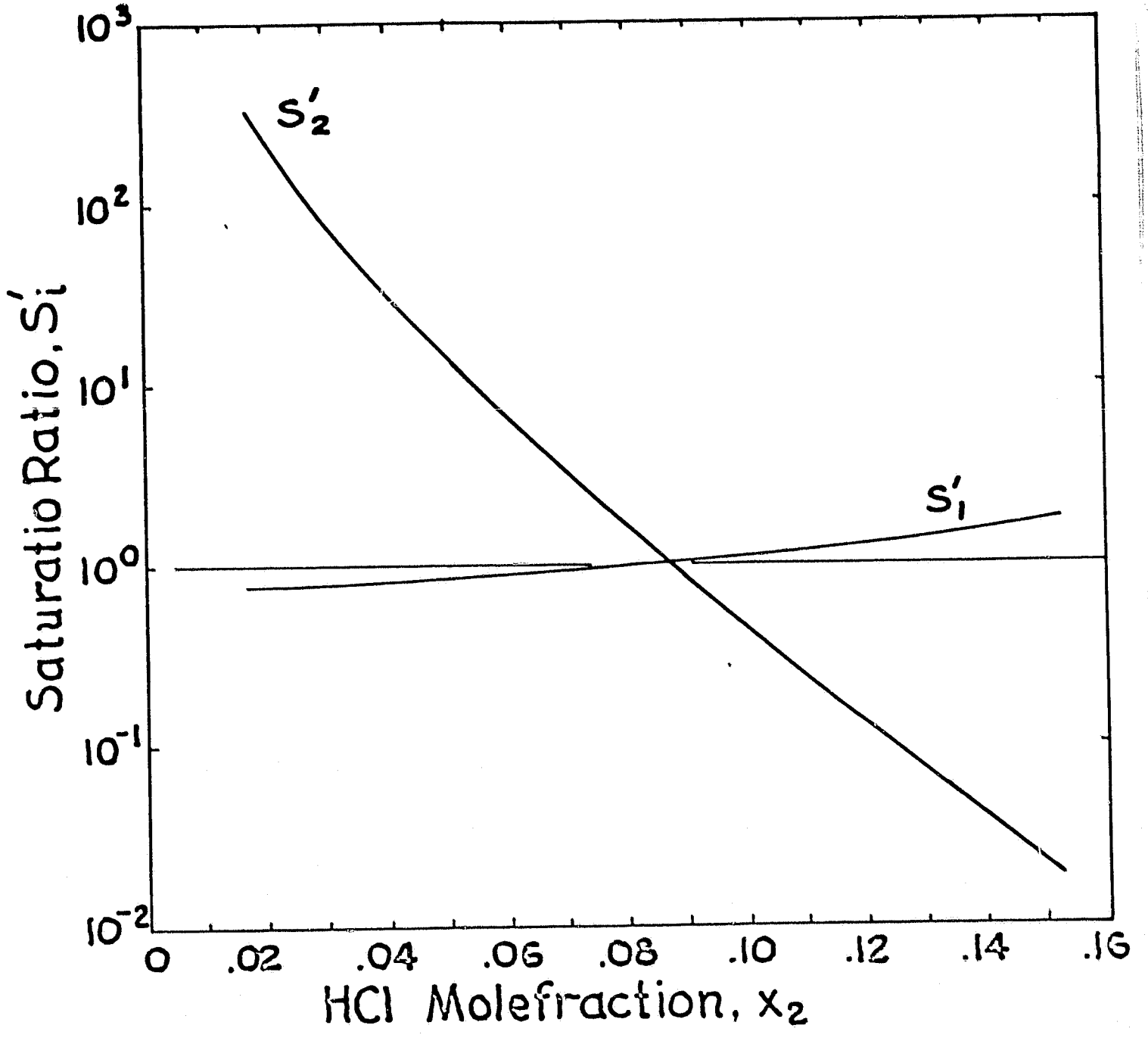

FIGURE 1.

defined by

$$\dot{r}_s \equiv \{\frac{3}{4\pi}\,[(1 - x_2)\,\dot{v}_i + x_2\,\dot{v}_2\,]\}^{1/3}$$

where $\dot{v}_1$ and $\dot{v}_2$ are respectively the molecular volumes of H_2O and HCl in solution. In general, the molecular volume of species i may be written

$$\dot{v}_i = M_i/\rho' n_0$$

giving

$$\dot{v}_1 = 2.9914 \times 10^{-23}\ (\frac{1}{\rho'})$$

and $\dot{v}_2 = \beta \dot{v}_1$.

Values of $\dot{r}_s$ for the concentration range $1.8 \times 10^{-5} \leq x_2 \leq 6.4306 \times 10^{-1}$ are given in Table 1.

Table 1. Values of $\dot{r}_s$ for HCl_{aq} in the concentration range $10^{-3} < M < 10^{2}$

x_2	M	x_1	$10^8 \cdot \dot{r}_s$ cm
1.8×10^{-5}	10^{-3}	0.999982	1.9256
1.8×10^{-4}	10^{-2}	0.00082	1.9259
1.8×10^{-3}	10^{-1}	0.9982	1.9269
1.77×10^{-2}	10^{0}	0.9823	1.9373
1.5266×10^{-1}	10^{1}	0.84734	2.0212
6.4306×10^{-1}	10^{2}	0.35694	2.2794

A reasonable value for $\dot{r}_s$ in the concentration range of $8 \times 10^{-2} \leq x_2 \leq 9 \times 10^{-2}$ is 2×10^{-8} cm. Using this value in (6b), $\dot{n}_1$ may be calculated, and ΔF may be determined as a function of r_p and x_2 for specified environmental conditions.

Taking environmental conditions as found in the stabilized ground cloud generated by a Titan III launch: $T = 298.16°K$, $P_1 = 23582$ dynes/cm^2. $P_2 = 104.5$ dynes/cm^2 at time $t = 90$ sec., the map of ΔF in (x_2, r_p) coordinates (Fig. 2) is constructed.

The contours of the ΔF surface in r_p, x_2 coordinates show a definite "saddle point", †, which for the specified environmental conditions, occurs at $r_p = 1.3 \times 10^{-6}$ cm, $x_2 = 8.8 \times 10^{-2}$. This point is analogous to the critical point defined for single vapor heterogeneous nucleation (see, e.g., Byers, 1965, Chap. 2). The surface thus defined is equivalent to the free energy surface $\Delta G\ (n_A, n_B)$ for the H_2O - H_2SO_4 system that has been discussed by Reiss (1950), Kiang and Stauffer (1973), Hamill (1975) and Hamill, et al (1977). Reiss (1950) showed that, when the surface energy term is included in the free energy expression, the free energy surface $\Delta G\ (n_A, n_B)$ is saddle-shaped with a saddle point defined by $\frac{\delta}{\delta n_A}(\Delta G) = 0$ and $\frac{\delta}{\delta n_B}(\Delta G) = 0$. The saddle shape was also found to be present under stratospheric conditions for the H_2O - H_2SO_4 system by Hamill, et al (1977).

Several features of the $\Delta F\ (x_2, r_p)$ surface (Figure 2) merit discussion. At constant $x_2 = 8.8 \times 10^{-2}$, ($M = 5.355$), the ΔF values rise gradually with increasing particle size in the range 10^{-8} cm $\leq r_p \leq 1.3 \times 10^{-6}$ cm, reaching a maximum of 25×10^{-11} erg at the latter

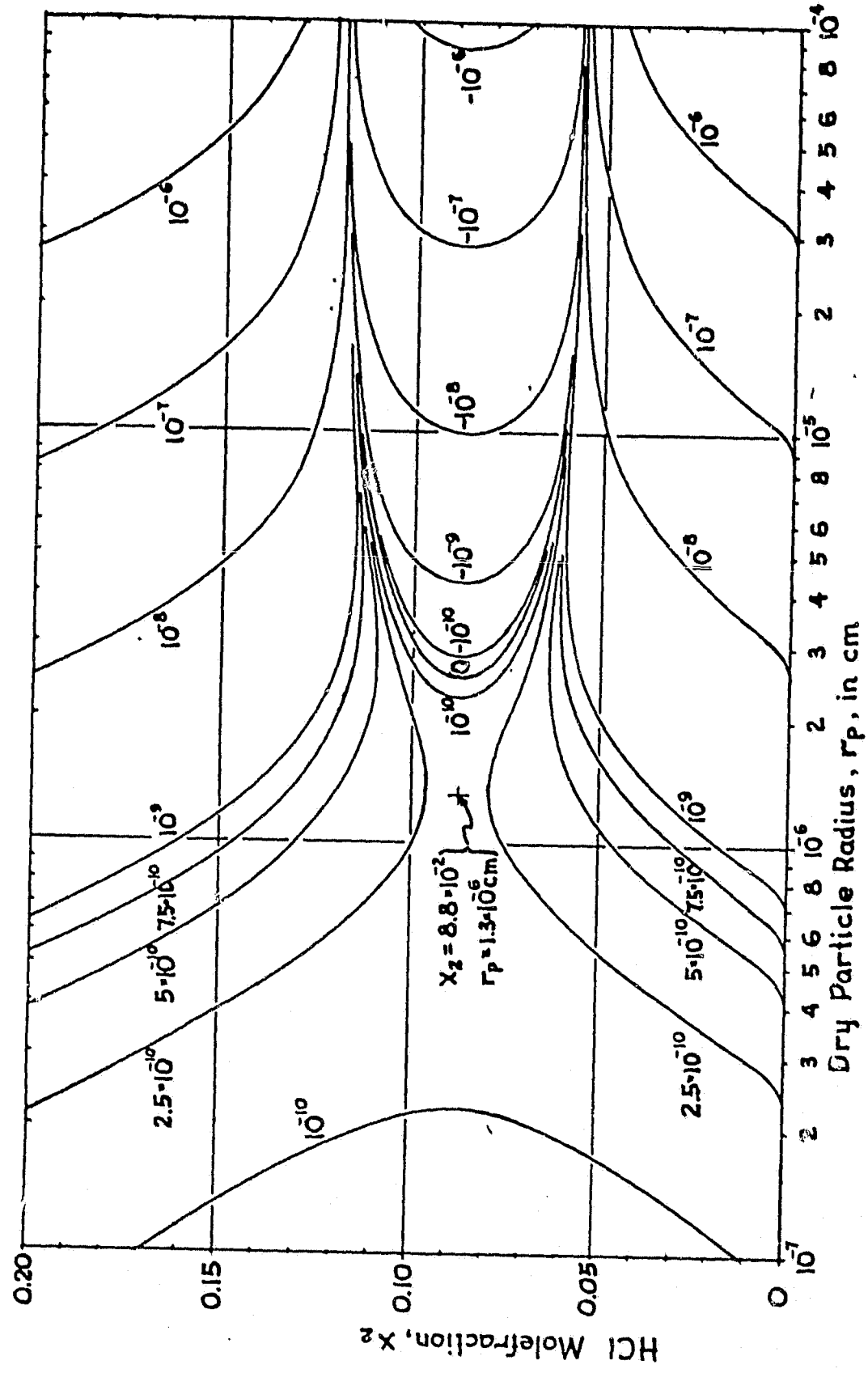

FIGURE 2.

size (saddle point). ΔF then decreases to 0 at $r_p = 2.67 \times 10^{-6}$ cm and decreases sharply to large negative values for larger sizes.

At higher and lower concentrations, e.g., $x_2 \geq 13 \times 10^{-2}$ and $x_2 \leq 4 \times 10^{-2}$, the ΔF surface rises sharply as r_p increases above 10^{-6} cm. Thus the growth region for HCl aq. droplets lies between nearly vertical "canyon" walls at $x_2 \sim 5.8 \times 10^{-2}$ and $x_2 \sim 11.7 \times 10^{-2}$ for nuclei of size $r_p \sim 2 \times 10^{-6}$cm and larger. The bottom of the "canyon" is relatively broad and flat with the locus of minima lying near $x_2 = 8.8 \times 10^{-2}$.

The profile of the ΔF (x_2, r_p) surface taken at $r_p = 10^{-5}$cm (Figure 3) shows the shape of the "canyon." In addition the values of the respective components of ΔF are shown for $r_p = 10^{-5}$cm as a matter of interest. This diagram necessarily is discontinuous at $\Delta F = 0$. The terms represented are:

$$\Delta F_\delta = 4\pi\sigma' (a^2 - r_p^2) \sim \text{constant}$$

$$\Delta F_1 = \dot{n}_1 \, k \, T \ln S_1'$$

$$\Delta F_2 = \dot{n}_2 \, k \, T \ln S_2'$$

$$\Delta F' = \Delta F_1 + \Delta F_2$$

$$\Delta F = \Delta F' + \Delta F_r$$

ΔF_2 is affected by two factors: (a) as x_2 increases, $\dot{n}_2$ also must increase, and (b) as x_2 increases S_2' must decrease causing $\ln S_2'$ to go from positive to negative values as S_2' decreases through 1.0. The result of this is a minimum in ΔF_2 near $x_2 = 4.5 \times 10^{-2}$, and a sign reversal near $x_2 = 8.8 \times 10^{-2}$. No minimum is found for ΔF_1 because both $\dot{n}_1$ and S_1' decrease as x_2 increases. Inasmuch as droplet growth cannot proceed unless both vapors are saturated, the curves ΔF_1 and ΔF_2 indicate that the region for droplet growth is in fact much narrower than the ΔF "canyon." This is true because, if

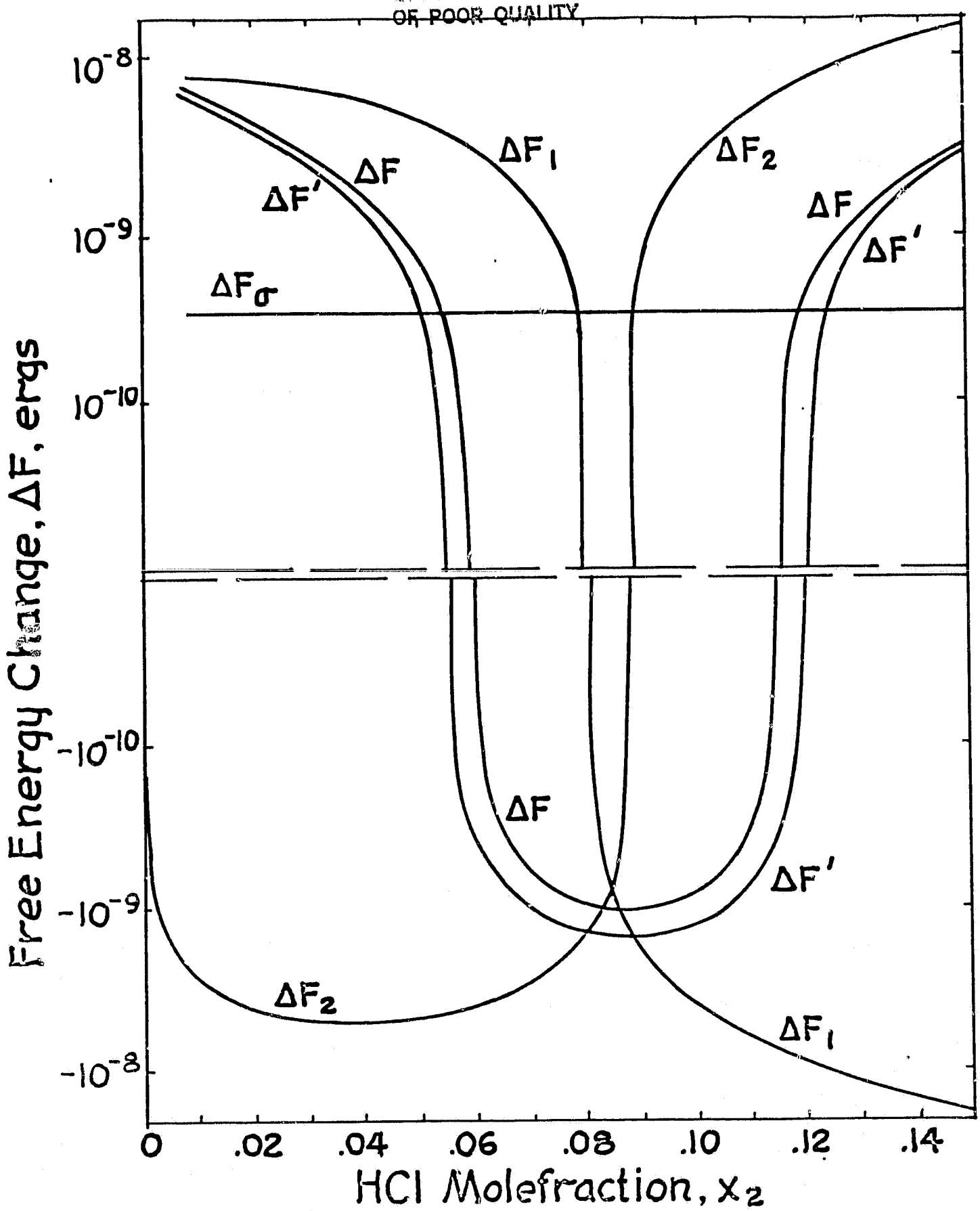

FIGURE 3.

either vapor is undersaturated, a droplet in that vapor must yield the undersaturated species by evaporation because the mass diffusion is proportional to $P_i(S_i'-1)$. The approximate range for nucleation to occur is $8.15 \times 10^{-2} \leq x_2 \leq 8.85 \times 10^{-2}$. The minimum value of ΔF occurs at $x_2 = 8.82 \times 10^{-2}$, thus this is the most probable HCl concentration for a particle size $r_p = 10^{-5}$cm under the specified conditions.

It is clear that ΔF (x_2, r_p) varies with T, P_1 and P_2. For the purposes of NASA, the maps of $\Delta F(x_2, r_p)$ for the various environmental conditions that may be encountered at different launch sites and in all seasons should be computed. Particularly the changes imposed upon the system by the increase of solid rocket booster capacity required for the Space Shuttle should be more completely evaluated.

III. An Explicit Mixed Numerical Method for Atmospheric Models

by

H-m Hsu

Assistant Professor of Atmospheric Science

University of Wisconsin, Milwaukee

Abstract

An explicit, mixed numerical method has been developed for atmospheric models. In a set of physical equations, the forward finite-difference scheme is applied for the time tendency terms, upstream for the advection terms, and central for other terms. For either the shallow-water equations in one or two dimensions or the primitive equations in three dimensions, the mixed method is conditionally stable and shows much better accuracy than that of the pure forward-upstream method. It is also shown that the traditional CFL condition is only a special case of the stability conditions revealed in this study.

1. Introduction

Numerical simulation has become a more and more important method to reveal atmosphere processes, because the traditional analytic method has frequently failed to provide solutions from complex systems of partial differential equations which describe atmospheric phenomena. Different numerical schemes are used to approximate such systems from differential form to difference form. Due to the limitation on computer resources, economy and accuracy of the numerical scheme should be simultaneously considered.

The central finite-difference scheme has been widely applied in atmospheric numerical models, and recently became so popular that one tends only to emphasize its advantage in higher-order accuracy of solution and de-emphasize its bad performance in actual calculations. In fact, this scheme not only generates erroneous small-scale perturbations which gradually distort the model results, but also provides two separate solutions for odd and even time-steps during the numerical integration. To avoid those errors, artificial space and time smoothers are necessary and have to be implemented into the computational algorithm. Among other explicit schemes, a lower-order scheme without any smoother may become an adequate alternative. After all, the central-differencing scheme (a three-time-level scheme) requires more programming efforts and greater computer resources than lower-order ones (i.e. two-time-level schemes).

The explicit two-time-level schemes used in atmospheric models have been described and summarized by Thompson (1), Mesinger and Arakawa (2) and Haltiner and Williams (3). For a single linear advection equation, the forward-in-time and upstream-in-space scheme has been proved to

be stable, whereas the forward-in-time and central-in-space is unstable. If a more complicated system than a simple advection equation is approximated by a mixed method, the stability of the approximate system cannot be safely determined without careful analysis. The mixed method considered here consists of the forward scheme for time tendency terms, the upstream scheme for advective terms, and the central scheme for other terms in the system.

The purpose of this paper is to demonstrate that the mixed method is conditionally stable for both linearized systems of shallow-water equations and primitive equations.

2. Linear shallow-water system

The shallow-water system is the simplest primitive equation system for an incompressible, hydrostatic, adiabatic and frictionless fluid. Kasahara (4) applied the central finite-difference scheme to a one-dimensional system with two different staggered grid-nets, and analyzed the numerical stabilities. From his study he indicated that stability analysis should not be performed separately for every physical factor in the system, but for the entire system instead. Same shallow-water equations will be adopted here to illustrate the numerical stability of the mixed method for those equations.

The one-dimensional shallow-water equations are

$$\frac{\partial u}{\partial t} + \bar{U} \frac{\partial u}{\partial x} + g \frac{\partial h}{\partial x} = 0 \qquad (1.a)$$

$$\frac{\partial h}{\partial t} + \bar{U}\frac{\partial h}{\partial x} + H\frac{\partial u}{\partial x} = 0 \qquad (1.b)$$

Symbols are defined in the Appendix. Basic properties of the mixed method may be revealed as follows.

a. Stability

Let u_ℓ^n denote the finite-difference approximation to $u(t,x) \equiv u(n\Delta t, \ell\Delta x)$ and define h_ℓ^n in a similar manner. The difference equations of (1) are

$$\frac{u_\ell^{n+1} - u_\ell^n}{\Delta t} + \bar{U}\frac{u_\ell^n - u_{\ell-1}^n}{\Delta x} + g\frac{h_{\ell+1}^n - h_{\ell-1}^n}{2\Delta x} = 0 \qquad (2.a)$$

and

$$\frac{h_\ell^{n+1} - h_\ell^n}{\Delta t} + \bar{U}\frac{h_\ell^n - h_{\ell-1}^n}{\Delta x} + H\frac{u_{\ell+1}^n - u_{\ell-1}^n}{2\Delta x} = 0 \qquad (2.b)$$

if $\bar{U} > 0$. Same set of finite difference equations is separately constructed by Brown and Pandolfo [5], and stability is analyzed in an uncoupled approach. The solutions are assumed to have the following form

$$\begin{Bmatrix} u_\ell^n \\ h_\ell^n \end{Bmatrix} = \begin{Bmatrix} \hat{u}^n \\ \hat{h}^n \end{Bmatrix} \exp\left[i\,(\alpha\,\ell\Delta x)\right] \qquad (3)$$

Substitute (3) into (2), and an amplification matrix is obtained (Richtmyer and Morton, (6)).

$$G = \begin{bmatrix} \psi - i\phi & -i\xi_x \\ -i\zeta_x & \psi - i\phi \end{bmatrix}, \tag{4}$$

where $\psi = 1 - \bar{U}\frac{\Delta t}{\Delta x}(1 - \cos \alpha\Delta x)$, (5)

$$\phi = \bar{U}\frac{\Delta t}{\Delta x} \sin \alpha\Delta x, \tag{6}$$

$$\xi_x = g\frac{\Delta t}{\Delta x} \sin \alpha\Delta x \tag{7}$$

and $\zeta_x = H\frac{\Delta t}{\Delta x} \sin \alpha\Delta x.$ (8)

The eigenvalues of the amplification matrix, G

are $\lambda = \psi - i\,(\phi + \sqrt{\xi_x \zeta_x})$, (9)

and $\lambda_* = \psi - i\,(\phi - \sqrt{\xi_x \zeta_x})$. (10)

While λ is the physical mode of the solution, λ_* is the computational mode. The squared absolute value of eigenvalue is

$$|\lambda|^2 = 1 - B\Delta t + A\Delta t^2 \tag{11}$$

where $$A = 2\left(\frac{\bar{U}}{\Delta x}\right)^2 (1-\cos \alpha\Delta x) + \left(\frac{C_g}{\Delta x}\right)^2 \sin^2 \alpha\Delta x \tag{12}$$

$$+ 2\frac{\bar{U}\, C_g}{(\Delta x)^2} \sin^2 \alpha\Delta x,$$

$$B = 2\left(\frac{\bar{U}}{\Delta x}\right) (1-\cos \alpha\Delta x), \tag{13}$$

and $$C_g = \sqrt{gH} \tag{14}$$

The von Neuman condition for stability (Richtmyer and Morton, (6)) requires that

$$|\lambda|^2 \leq 1. \tag{15}$$

Combining (11) and (15), a stability criterion is arrived,

$$\Delta t \leq \frac{B}{A} \tag{16}$$

This concludes that the mixed numerical method is <u>conditionally stable</u> for a linearized one-dimensional shallow-water system.

Theoretically, the stability bound can be reached asymptotically,

$$\Delta t_* = \frac{\bar{U}\,\Delta x}{(\bar{U} + C_g)^2} \tag{17}$$

as the wave number of a single Fourier component approaches to zero. Obviously, in term of velocity $\bar{U}$, there is a maximum of the asymptotic stability bound for different depth of fluid. Figure 1 shows the variations of Δt_* for different depths of fluid and horizontal increments under certain wind regime. If there is no surface gravity wave ($H = 0$), the CFL (Courant-Friedrichs-Lewy) condition is met, and Δt_* decreases monotonically as $\bar{U}$ increases (Fig. 1a). For slow-moving waves, Δt_* increases with increasing velocity, then decreases after it passes its maximum (Fig. 1b and c). Finally, Δt_* will reach zero as $\bar{U}$ approaches to infinite. For fast-moving waves, the maximum of $\bar{U}$ is beyond 20 m/sec, and Δt_* decreases with decreasing velocity monotonically to zero (Fig. 1d and 1e).

The CFL Condition (Fig. 1a) is only a special case in the present results which give opposite conditions (e.g. Fig. 1d and 1e) to the CFL conditions in certain situations ($H = 100$m and 1000m, respectively). It is also observed that for the shallower fluid Δt_* is dominated by the fluid velocity, and for the deeper fluid Δt_* primarily depends on the speed of surface gravity wave.

The maxima for Δt_* and $\bar{U}$ can easily be determined, and they are

$$\bar{U}_{max} = C_g, \tag{18}$$

and

$$\Delta t_{max} = \frac{1\,\Delta x}{4\,C_g}. \tag{19}$$

Hence, it is concluded that Δt_{max} is inversely proportional to the

speed of surface gravity waves. In other words, the deeper the fluid, the shorter the time-step.

There are two special cases and they may be described as follows,

Case 1: If $C_g = 0$, (11) becomes

$$|\lambda|^2 = 1 - 2\left(\frac{\bar{U}}{\Delta x}\right)(1 - \cos \alpha\Delta x)\,\Delta t + 2\left(\frac{\bar{U}}{\Delta x}\right)^2 (1 - \cos \alpha\Delta x)\,\Delta t^2. \tag{20}$$

Thus $$\Delta t \leq \frac{\Delta x}{\bar{U}} \tag{21}$$

is the conditional stability criterion for the pure forward-upstream method applied to the simple advection equation. For simplicity this method is called pure method, which was heavily criticized by Moelnkamp (7) because of its highly dissipative character.

Case 2: If $\bar{U} = 0$, (11) becomes

$$|\lambda|^2 = 1 + \left(C_g \frac{\Delta t}{\Delta x} \sin \alpha\Delta x\right)^2. \tag{22}$$

$|\lambda|^2$ is always greater than unity, and this method is absolutely unstable. Hence, $\bar{U}$ is not allowed to vanish.

b. Damping factor

The absolute value of the eigenvalue for the physical mode is a good indicator to compare how much the original wave amplitudes are reduced by the truncation errors due to different finite-difference methods. For the mixed method, $|\lambda|^2$ is described in (11). For the pure method, the third terms in both (2a) and (2b) are approximated by the upstream-in-

space scheme rather than by the central-in-space one, then we have

$$|\lambda|^2 = 1 - 2\left[1 - (\bar{U}+C_g)\frac{\Delta t}{\Delta x}\right](\bar{U}+C_g)\left(\frac{\Delta t}{\Delta x}\right)(1-\cos\alpha\Delta x), \qquad (23)$$

following the same mathematical procedure to obtain (11). The stability criterion is immediately provided,

$$\Delta t \leq \frac{\Delta x}{\bar{U} + C_g}. \qquad (24)$$

To show the comparison of the damping factors between these methods, $|\lambda|^2$ is plotted against Δt for nine waves. In general, the time step for a stable calculation is more restrictive for the mixed method (Fig. 2) than that for the pure method (Fig. 3). However, $|\lambda|^2$ gives remarkably less damping for the mixed method than that for the pure method. For example, the least $|\lambda|^2$ for $5\Delta x$ wave is greater than 99.5 5% for the mixed method, and is about 75% for the pure method. The high accuracy of the mixed method is obvious. Another interesting point is that the time step decreases with increasing wavelength for the mixed method, while it is a constant for the pure method. The indication is that an accurate representation of wave requires short time step and the truncation errors due to foreward-in-time difference scheme is greatly reduced. Over all, it is concluded that the mixed method is more accurate even though relatively small time increments are necessary. Also, the mixed method demands the same programing efforts and computer resources as the pure method does, but much less than the leap-frog method.

c. Phase speed

The false computational dispersion associated with a finite-difference

method usually distorts the true solution of the problem. The acceleration and retardation of the approximate solution from a set of finite-difference equations can be described by the phase speed of the physical mode. The true phase speed of the one-dimensional shallow-water system is $(\bar{U} + C_g)$. After thorough analysis, the phase speeds of different approximations in space for this system are the same, i.e., $(\bar{U} + C_g) \frac{\sin \alpha\Delta x}{\alpha\Delta x}$ among the mixed, pure, and leap-frog methods. Apparently, the true solution is generally retarded by any one of the approximations. In other words, the computational dispersion of the mixed method is as good as the leap-frog or pure method.

d. Two-dimensional case

For a two-dimensional shallow-water system, the Coriolis effect may be incorporated. The system consists of the following equations,

$$\frac{\partial u}{\partial t} + \bar{U} \frac{\partial u}{\partial x} + \bar{V} \frac{\partial u}{\partial y} + g \frac{\partial h}{\partial x} - fv = 0, \tag{25.a}$$

$$\frac{\partial v}{\partial t} + \bar{U} \frac{\partial v}{\partial x} + \bar{V} \frac{\partial v}{\partial y} + g \frac{\partial h}{\partial y} + fu = 0 \tag{25.b}$$

$$\frac{\partial t}{\partial h} + \bar{U} \frac{\partial h}{\partial x} + \bar{V} \frac{\partial h}{\partial y} + H \left(\frac{\partial u}{\partial x} + \frac{\partial v}{\partial y}\right) = 0 \ . \tag{25.c}$$

The mixed method is applied to this system except u and v in the Coriolis terms are approximated by $u^n_{\ell,m}$ and $v^n_{\ell,m}$ respectively. The two-dimensional stability criterion for the difference system is

$$\Delta t \leq \frac{B}{A}, \tag{26}$$

where

$$A = 2\left(\frac{\bar{U}}{\Delta x}\right)^2 (1-\cos \alpha\Delta x) + 2\left(\frac{\bar{V}}{\Delta y}\right)^2 (1-\cos \beta\Delta y)$$

$$+ 2 \frac{\bar{U}}{\Delta x} \frac{\bar{V}}{\Delta y} \; 1-\cos \alpha\Delta x - \cos \beta\Delta y + \cos(\alpha\Delta x - \beta\Delta y)$$

$$+ (f^2 + C_g^2 \delta^2) \qquad (27)$$

$$+ 2\left(\frac{\bar{U}}{\Delta x} \sin \alpha\Delta x + \frac{\bar{V}}{\Delta y} \sin \beta\Delta y\right) (f^2 + C_g^2 \delta^2)^{\frac{1}{2}},$$

$$B = 2 \; \frac{\bar{U}}{\Delta x} (1-\cos \alpha\Delta x) + \frac{\bar{V}}{\Delta y} (1-\cos \beta\Delta y) \quad , \qquad (28)$$

and $$\delta^2 = \frac{\sin^2 \alpha\Delta x}{\Delta x^2} + \frac{\sin^2 \beta\Delta y}{\Delta y^2} \quad , \qquad (29)$$

if the solutions have the form

$$\begin{Bmatrix} u^n_{\ell,m} \\ v^n_{\ell,m} \\ h^n_{\ell,m} \end{Bmatrix} = \begin{Bmatrix} \hat{u}^n \\ \hat{v}^n \\ \hat{h}^n \end{Bmatrix} \exp\left[i\,(\alpha\ell\Delta x + \beta m\Delta y)\right] \; . \qquad (30)$$

It is clear that the Coriolis effect is dominated by the surface gravity waves, if the fluid is deep enough. The basic properties of

this two-dimensional approximation is quite similar to the previous one-dimensional one.

3. Linear primitive-equation: A three-dimensional system

To model atmospheric phenomena in mesoscale, a more complete set of coupled primitive equations than a shallow water system is clearly needed. Careful analysis of numerical stability for the approximate system is necessary to ensure stable calculations. The linear primitive equations which will be used here are the simplifications of a three-dimensional mesoscale model equations (Hsu, (8)). They are

$$\frac{\partial u}{\partial t} + \bar{U}\frac{\partial u}{\partial x} + \bar{V}\frac{\partial u}{\partial y} + \theta_o \frac{\partial \pi}{\partial x} - fv - K\frac{\partial^2 u}{\partial z^2} = 0, \tag{31.a}$$

$$\frac{\partial v}{\partial t} + \bar{U}\frac{\partial v}{\partial x} + \bar{V}\frac{\partial v}{\partial y} + \theta_o \frac{\partial \pi}{\partial y} + fu - K\frac{\partial^2 v}{\partial z^2} = 0, \tag{31.b}$$

$$\theta_o \frac{\partial \pi}{\partial z} - \frac{g}{\theta_o}\theta = 0, \tag{31.c}$$

$$\frac{\partial u}{\partial x} + \frac{\partial v}{\partial y} + \frac{\partial w}{\partial z} = 0, \tag{31.d}$$

$$\frac{\partial \theta}{\partial t} + \bar{U}\frac{\partial \theta}{\partial x} + \bar{V}\frac{\partial \theta}{\partial y} + wS - K\frac{\partial^2 \theta}{\partial z^2} = 0 \tag{31.e}$$

a. Stability

Let $A^n_{\ell,m,k}$ denote the finite-difference approximation to $A(t,x,y,z) \equiv A(n\Delta t, \ell\Delta x, m\Delta y, k\Delta z)$ for the dependent variables u, v, w, π, and θ. The finite-difference equations of the mixed method are

$$\frac{u^{n+1} - u^n}{\Delta t} + \bar{U}\frac{u_\ell - u_{\ell-1}}{\Delta x} + \bar{V}\frac{u_m - u_{m-1}}{\Delta y} + \theta_0\frac{\pi_{\ell+1} - \pi_{\ell-1}}{2\Delta x} - fv^n - K\frac{u_{k+1} - 2u_k + u_{k-1}}{\Delta z^2} = 0, \tag{32.a}$$

$$\frac{v^{n+1} - v^n}{\Delta t} + \bar{U}\frac{v_\ell - v_{\ell-1}}{\Delta x} + \bar{V}\frac{v_m - v_{m-1}}{\Delta y} + \theta_0\frac{\pi_{m+1} - \pi_{m-1}}{2\Delta y} + fu^n - K\frac{v_{k+1} - 2v_k + v_{k-1}}{\Delta z^2} = 0, \tag{32.b}$$

$$\theta_0\frac{\pi_{k+1} - \pi_k}{\Delta z} - \frac{g}{\theta_0}\frac{\theta_{k+1} + \theta_k}{2} = 0, \tag{32.c}$$

$$\frac{u_{\ell+1} - u_{\ell-1}}{2\Delta x} + \frac{v_{m+1} - v_{m-1}}{2\Delta y} + \frac{w_{k+1} - w_{k-1}}{2\Delta z} = 0, \tag{32.d}$$

and

$$\frac{\theta^{n+1} - \theta^n}{\Delta t} + \bar{U}\frac{\theta_\ell - \theta_{\ell-1}}{\Delta x} + \bar{V}\frac{\theta_m - \theta_{m-1}}{\Delta y} - Sw^n - K\frac{\theta_{k+1} - 2\theta_k + \theta_{k-1}}{\Delta z^2} = 0, \tag{32.e}$$

when we assume that $\bar{U} > 0$, and $\bar{V} > 0$.

Wave solutions of (32) take the form

$$A^{n}_{\ell,m,k} = \hat{A} \exp\{i(\alpha\ell\Delta x+\beta m\Delta y+\gamma k\Delta z)\}. \tag{33}$$

After substituting (33) into (32) and performing some algebraic manipulations, an amplification matrix can be obtained,

$$G = \begin{bmatrix} \psi-i\phi & f\Delta t & -\xi_x \\ -f\Delta t & \psi-i\phi & -\xi_y \\ \zeta_x & \zeta_y & \psi-i\phi \end{bmatrix} \tag{34}$$

where

$$\psi = 1 - \bar{U}\frac{\Delta t}{\Delta x}(1 - \cos\alpha\Delta x) - \bar{V}\frac{\Delta t}{\Delta y}(1 - \cos\beta\Delta y) + 2\frac{K\Delta t}{\Delta z^2}(1 - \cos\gamma\Delta z), \tag{35}$$

$$\phi = \bar{U}\frac{\Delta t}{\Delta x}\sin\alpha\Delta x + \bar{V}\frac{\Delta t}{\Delta y}\sin\beta\Delta y, \tag{36}$$

$$\xi_x = \frac{g\,\Delta t}{\theta_0}\frac{\Delta z}{\sin\gamma\Delta z}\frac{\sin\alpha\Delta x}{\Delta x}, \tag{37}$$

$$\xi_y = \frac{g\,\Delta t}{\theta_0}\frac{\Delta z}{\sin\gamma\Delta z}\frac{\sin\beta\Delta y}{\Delta y}, \tag{38}$$

$$\zeta_x = S\,\Delta t\frac{\Delta z}{\sin\gamma\Delta z}\frac{\sin\alpha\Delta x}{\Delta x}, \tag{39}$$

and

$$\zeta_y = S\,\Delta t\frac{\Delta z}{\sin\gamma\Delta z}\frac{\sin\beta\Delta y}{\Delta y}. \tag{40}$$

The physical eigenvalue of the amplification matrix is

$$\lambda = \psi - i\{\phi + (\xi_x\zeta_x + \xi_y\zeta_y + f^2\Delta t^2)^{\frac{1}{2}}\}. \tag{41}$$

The squared absolute value of λ is

$$|\lambda|^2 = 1 - B\Delta t + A\Delta t^2, \tag{42}$$

where

$$A = 2(\frac{\bar{U}}{\Delta x})^2(1 - \cos\alpha\Delta x) + 2(\frac{\bar{V}}{\Delta y})^2(1 - \cos\beta\Delta y)$$

$$+ 2\,\frac{\bar{U}}{\Delta x}\,\frac{\bar{V}}{\Delta y}\{1 - \cos\alpha\Delta x - \cos\beta\Delta y + \cos(\alpha\Delta x - \beta\Delta y)\}$$

$$+ 2(\frac{\bar{U}}{\Delta x}\sin\alpha\Delta x + \frac{\bar{V}}{\Delta y}\sin\beta\Delta y)(N^2\delta^2 + f^2)^{\frac{1}{2}}$$

$$+ (N^2\delta^2 + f^2)$$

$$+ 4\{1 - \frac{\bar{U}}{\Delta x}(1 - \cos\alpha\Delta x) - \frac{\bar{V}}{\Delta y}(1 - \cos\beta\Delta y)\}$$

$$\{\frac{K}{\Delta z^2}(1 - \cos\gamma\Delta z)\}$$

$$+ 4\,\frac{K^2}{\Delta z^4}(1 - \cos\gamma\Delta z)^2, \tag{43}$$

$$B = 2\,\frac{\bar{U}}{\Delta x}(1 - \cos\alpha\Delta x) + 2\,\frac{\bar{V}}{\Delta y}(1 - \cos\beta\Delta y), \tag{44}$$

$$\delta^2 = \frac{\Delta z^2}{2(1 - \cos \gamma \Delta z)} \left(\frac{\sin^2 \alpha \Delta x}{\Delta x^2} + \frac{\sin^2 \beta \Delta y}{\Delta y^2} \right) \tag{45}$$

and $$N^2 \equiv \frac{g}{\theta_0} S \equiv \frac{g}{\theta_0} \frac{d\theta_0}{dz}. \tag{46}$$

Then the stability criterion is given in the von Neumann's sense,

$$\Delta t \leq \frac{B}{A}. \tag{47}$$

For this three-dimensional primitive -equation system, the mixed method is conditionally stable.

Since $\bar{U} = \bar{V} = 0$, $|\lambda|^2 > 1$. This method becomes absolutely unstable, so $\bar{U}$ or $\bar{V}$ is not allowed to vanish.

b. Averaging in the hydrostatic equation

The averaging procedure appears in (32.c), and is crucial to the stability of the approximate system. If θ in (31.c) has not been averaged, we may instead have

$$\theta_0 \frac{\pi_{k+1} - \pi_{k-1}}{2\Delta z} - \frac{g}{\theta_0} \theta^n = 0. \tag{48}$$

The only affected term in (42) is (45) and becomes

$$\delta^2 = \frac{\Delta z^2}{\sin^2 \gamma \Delta z} \left(\frac{\sin^2 \alpha \Delta x}{\Delta x^2} + \frac{\sin^2 \beta \Delta y}{\Delta y^2} \right). \tag{49}$$

For $2\Delta z$ wave, δ^2 is unbounded, and $|\lambda|^2$ is much greater than 1. Hence

the unstable situation occurs due to the inproper approximation of the hydrostatic equation.

c. Influences of physical factors

Generally, the relationship between $\bar{U}$ (or $\bar{V}$) and Δt in the primitive-equation systems still remains quite similar to that in the shallow-water system, because the same numerical technique is employed. However, two systems describe different physical waves, i.e. surface gravity waves for the shallow-water system and internal gravity waves for the primitive-equation system.

In the present primitive-equation system, three physical factors govern the stability bound and they are

(1) The Coriolis effect ($K = N = 0$)
(2) The thermal stratification ($\Phi = K = 0$), and
(3) The vertical diffusion ($N = \Phi = 0$).

When any one of these three factors is retained in the system Δt will have a maximum with respect to $\bar{U}$ (or $\bar{V}$). They are illustrated in figures (4a), (4b), and (4c) for the case (1) - $\Phi = 40^{\circ}$, case (2) - $N = 0.01$ sec^{-1}, and case (3) - $K = 10^3$ cm^2 sec^{-1}, respectively.

Δt decreases from its maximum to zero as $\bar{U}$ (or $\bar{V}$) either increases to infinite or decreases to zero. These results are different from the case which none of the physical factors appears in the system ($\Phi = K = N = 0$). In figure (4d), Δt is inversely proportional to $\bar{U}$ (or $\bar{V}$), and Δt is unbounded as $\bar{U}$ (or $\bar{V}$) goes to zero (i.e. the CFL condition).

Usually, Δt increases as Δx (Δy) increases. It can be found in figures (4b) and (4d). Both in figure (4a) and (4c), Δt increases as Δx (or Δy) decreases under weak $\bar{U}$ (or $\bar{V}$) conditions. It implies that under some situations, the shorter the horizontal increment, the larger

the time increment. This is quite unusual. In applications, Δt should be determined by exact calculation of (47).

d. Vertical dependence

The vertical dependence of the stability bound appears in the thermal stratification and vertical diffusion terms in (43). The limiting condition of that both the vertical increment and the vertical wavelength approach to zero provides the same result as eliminating the thermal stratification ($N = 0$) and the vertical diffusion ($K = 0$) effects (Fig. 4a).

If only the vertical diffusion effect is omitted in (43), the maximum time step decreases as the vertical increment and the vertical wavelength increase (Fig. 5a). This means that the shorter the vertical increment, the larger the time step. High accuracy in vertical with a long time step is obviously allowable. The situation becomes completely opposite when only the thermal stratification effect is not considered (Fig. 5b). While both effects are retained in the primitive equation system (Fig. 5c), it seems that the stability bound of a pure thermal stratification case (Fig. 5a) is modified by the vertical diffusion effect. Furthermore, for longer waves the modification of time increment by the vertical diffusion is weaker than that for the shorter waves. The reduction of time step is quite significant for short wavelength and short vertical increment.

e. Accuracy

In general, the accuracy of the mixed method applied to the three-dimensional primitive-equation system is quite good. Figure 6 shows the plot of $|\lambda|^2$ vs. Δt at $N = 0.01\ \text{sec}^{-1}$, $K = 10^3\ \text{cm}^2\ \text{sec}^{-1}$, $\Phi = 40^\circ$, $\bar{U} = \bar{V} = 10\ \text{m sec}^{-1}$, $10\ \Delta x$, $10\ \Delta y$ and $\Delta x = \Delta y = 30$ km. The lowest value of $|\lambda|^2$ is 97.63% (i.e. $|\lambda| = 98.81\%$) for the $6\Delta z$ waves. This very

weak damping may be very helpful to suppress the instability caused by non-linear integration.

4. Conclusion

A mixed numerical method has been developed for atmospheric models, and consists of the forward difference scheme for time tendency terms, the upstream scheme for advection terms, and the central scheme for other terms in a physical system. For simple advection equation, the forward-upstream method is excessively dissipative, while the forward-central one is absolutely unstable. The mixed method is a combination of these two methods. Most importantly, this method is conditionally stable and highly accurate to the approximate system of either the shallow-water equations in one or two dimensions or the primitive equations in three dimensions. The dependences of determining the stability bounds are not quite obvious. However, the analytic expressions of the linear stability criteria are given. Δt should be easily found under typical conditions. The traditional CFL criterion is only a special case of the present results, which give opposite criterion to the CFL criterion in certain situations.

The mixed method not only conserves computer resources but also programming efforts, because it is explicit and two-time-level. This method has been successfully applied by the author in his mesoscale model (Hsu, (8). Stable calculations have been achieved without any artificial spatial smoother or temporal filter.

To compare the accuracy of the model results among the mixed method and other explicit ones for a non-linear atmospheric model, it is necessary to simulate some real cases with different methods and analyze the differences between observational and computational data. This

effort is being undertaken. Implicit or semi-implicit method (e.g. Sun, (9) may be helpful to increase the length of the allowable time step for long-term integration.

Acknowledgments. The author would like to thank Mr. H.-K. Albert Lin for drafting the figures and Mrs. Donna Bobst for typing the manuscript. The research was partially supported by NASA-Langley under Grant NSG-1243 through the University of Michigan and by NOAA-ERL under Grant NA81RA00001 through the University of Wisconsin-Milwaukee.

Appendix List of Symbols

C_g	$\sqrt{gH}$, speed of surface gravity wave
f	$2\Omega\sin\Phi$, Coriolis parameter
g	gravitational acceleration
G	amplification matrix
h	height perturbation of a free surface
H	constant height of a free surface
i	$\sqrt{-1}$
K	vertical eddy exchange coefficient
ℓ, m, k	number of increments in x-, y-, and z- directions, respectively
N	$(\frac{g}{\theta_o}\frac{d\theta_o}{dZ})^{\frac{1}{2}}$, Brunt-Väisälä frequency
S	$\frac{d\theta_o}{dZ}$, constant potential temperature lapse rate
t	time
u, v, w	x-, y-, and z- components of velocity perturbation, respectively
$\bar{U}$, $\bar{V}$	constant velocities in x- and y- directions, respectively
$\bar{U}_{max}$	value of $\bar{U}$ corresponding to Δt_{max}
x, y, z	Cartesian coordinate
α, β, γ	wavenumbers in x-, y-, and z- directions, respectively .
Δt	time increment
Δt_*	limiting Δt as the wave number approaching to zero
Δt_{max}	maximum of Δt_*

Δx, Δy, Δz	space increments in x-, y-, and z- directions, respectively
θ	potential temperature perturbation
θ_o	constant potential temperature
λ	eigenvalue of the amplification matrix
π	scaled pressure perturbation
Φ	latitude
Ω	Earth rotation rate

References

1. Thompson, P.D., "Numerical Weather Analysis and Prediction", Macmillan, New York, 1961.

2. Mesinger, F., and A. Arakara, "Numerical Methods Used in Atmospheric Models, V.I.", GARP No. 17, World Meteorological Organization, UNIPUB, New York, 1976.

3. Haltiner, G.J., and R.T. Williams, "Numerical Prediction and Dynamic Meteorology", 2nd. ed., Wiley, New York, 1980.

4. Kasahara, A., Mon. Wea. Rev., 93, (1965), 27-31.

5. Brown, P.S., Jr., and J.P. Pandolfo, J. of Computational Physics, 36, (1980), 141-150.

6. Richtmyer, R.D., and K.W. Morton, "Difference Methods for Initial-Value Problems", 2nd. ed., Interscience, New York, 1967.

7. Molenkamp, C.R., J. Appl. Meteor., 1, (1968), 160-167.

8. Hsu, H.-m., "Numerical Simulations of Mesoscale Precipitation Systems", Ph.D. dissertation, The Univeristy of Michigan, Ann Arbor, Michigan, 1979.

9. Sun, W.Y., Mon. Wea. Rev., 108, (1980), 402-417.

FIGURE LEGENDS

Figure 1: Variations of Δt_{*} with respect to $\bar{U}$ for (a) H = 0, (b) H = 1 m, (c) H = 10 m, (d) H = 100 m, and (e) H = 1000 m. Curve lables are Δx in 10 km.

Figure 2: Damping factor $|\lambda|^2$ of the mixed method for (a) $2\Delta x - 4\Delta x$ waves and (b) $4\Delta x - 10\Delta x$ waves (Δx = 30 km, $\bar{U}$ = 10 m-sec^{-1}, and H = 1000 m).

Figure 3: Damping factor $|\lambda|^2$ of the pure method for $2\Delta x - 10\Delta x$ waves (x = 30 km, $\bar{U}$ = 10 m-sec^{-1}, and H = 1000 m).

Figure 4: Variations of Δt with respect to either $\bar{U}$ or $\bar{V}$ for (a) K = 0, N = 0, Φ_1 = 40°, (b) K = 0, N = 0.01 sec^{-1}, Φ = 0, (c) K = 10^3 cm^2-sec^{-1}, N = 0, Φ = 0, and (d) K = 0, N = 0, Φ = 0 for $10\Delta x$-$10\Delta y$-$5\Delta z$ wave (Δz = 1 km). Curve lables are Δx=Δy in km.

Figure 5: Variations of Δt with different vertical (Δz) waves for (a) K = 0, N = 0.01 sec^{-1}, (b) K = 10^3 cm^2-sec^{-1}, N = 0, and (c) K = 10^3 cm^2-sec^{-1}, N = 0.01 sec^{-1}. Horizontal constants are $10\Delta x$=$10\Delta y$ waves with Δx=Δy= 30 km, Φ = 40°, and $\bar{U}$=$\bar{V}$= 10 m-sec^{-1}. Curve lables are Δz in km.

Figure 6: Damping factor $|\lambda|^2$ of the mixed method in the three-dimensional mesoscale model for different vertical (Δz) waves. Constants are $10\Delta x$=$10\Delta y$ waves with Δx=Δy = 30 km, $\bar{U}$ = $\bar{V}$ = 10 cm-sec^{-1}, Φ = 40°, K = 10^3 cm^2-sec^{-1}, and N = 0.01 sec^{-1}.

Fig. 1

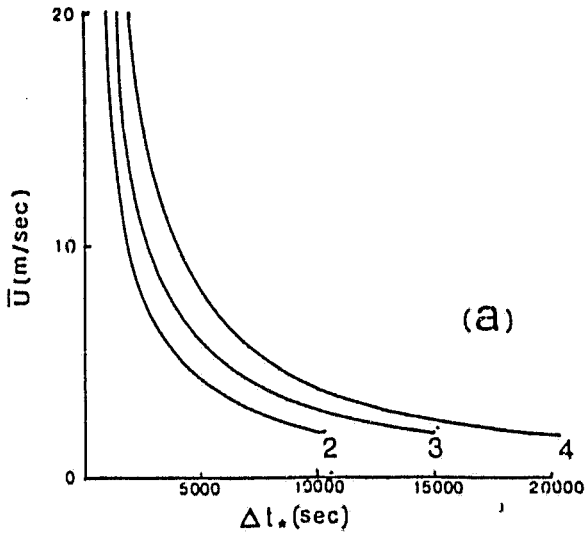

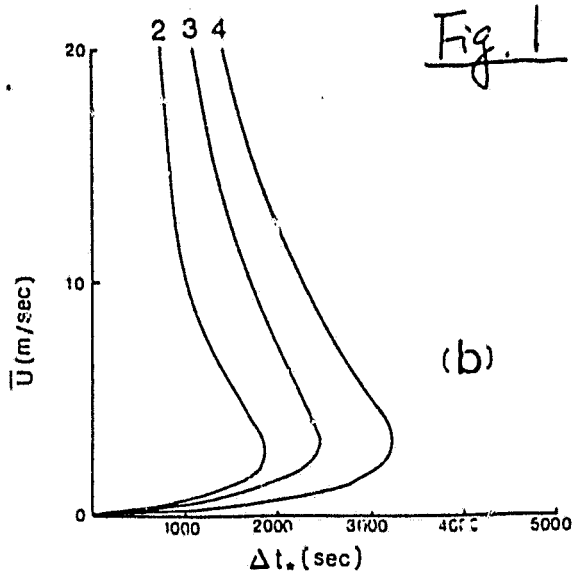

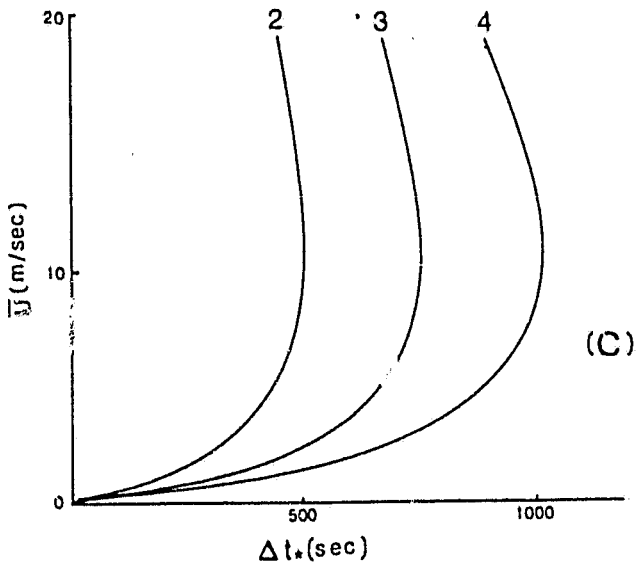

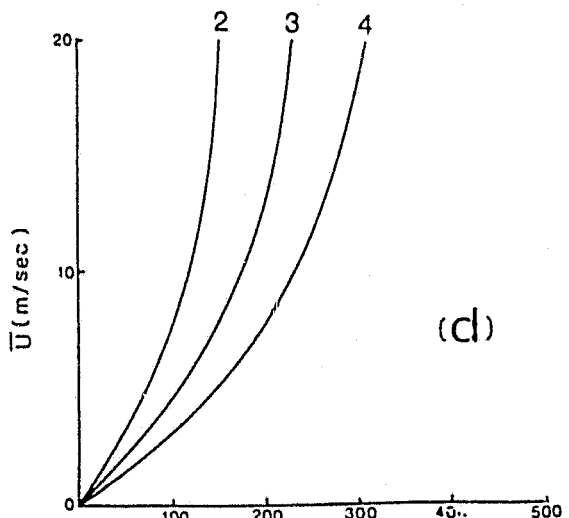

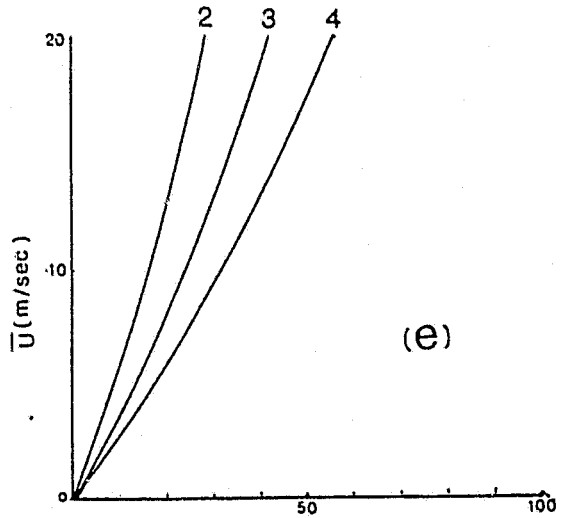

Fig 2a

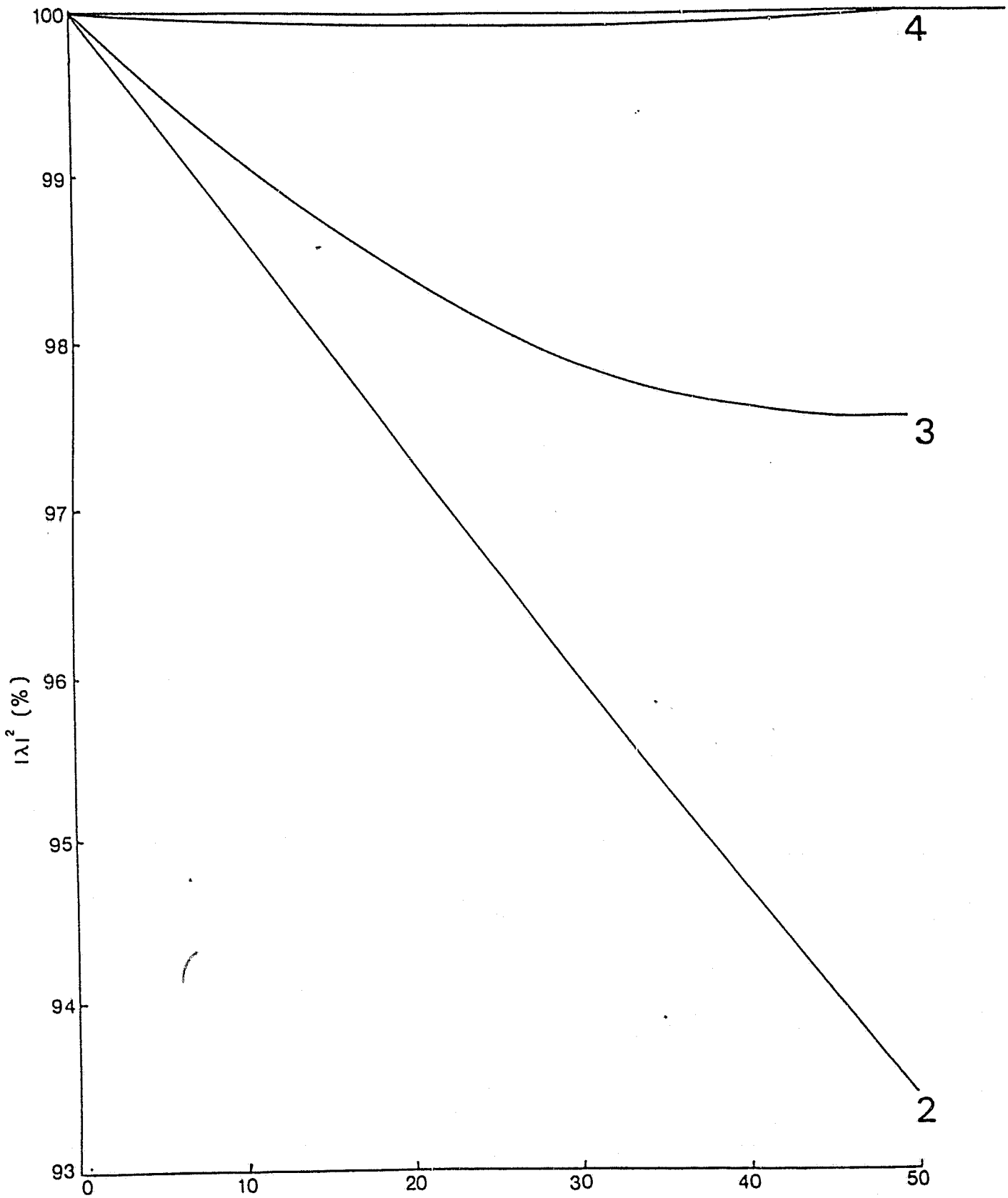

Fig. 2b

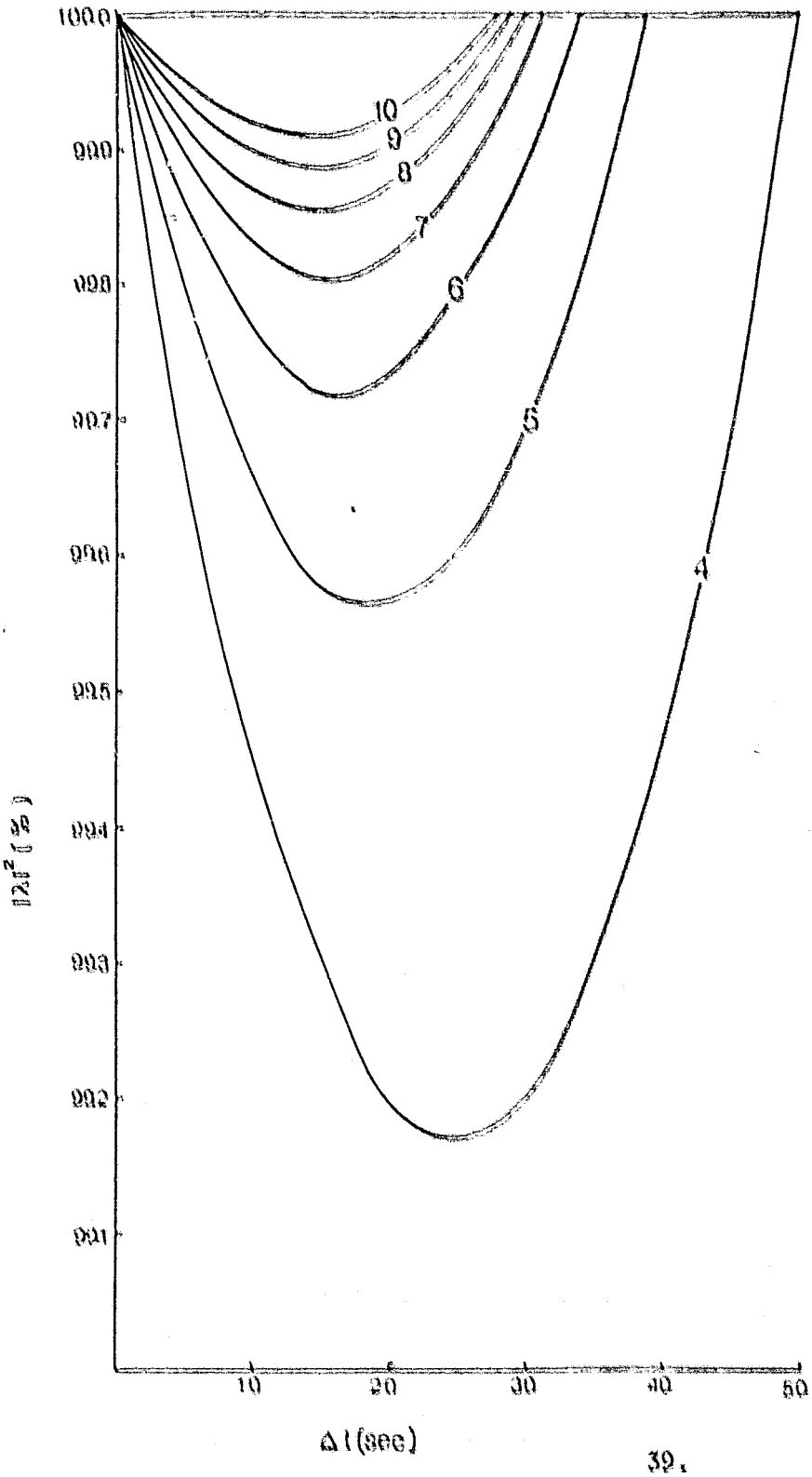

Fig. 3

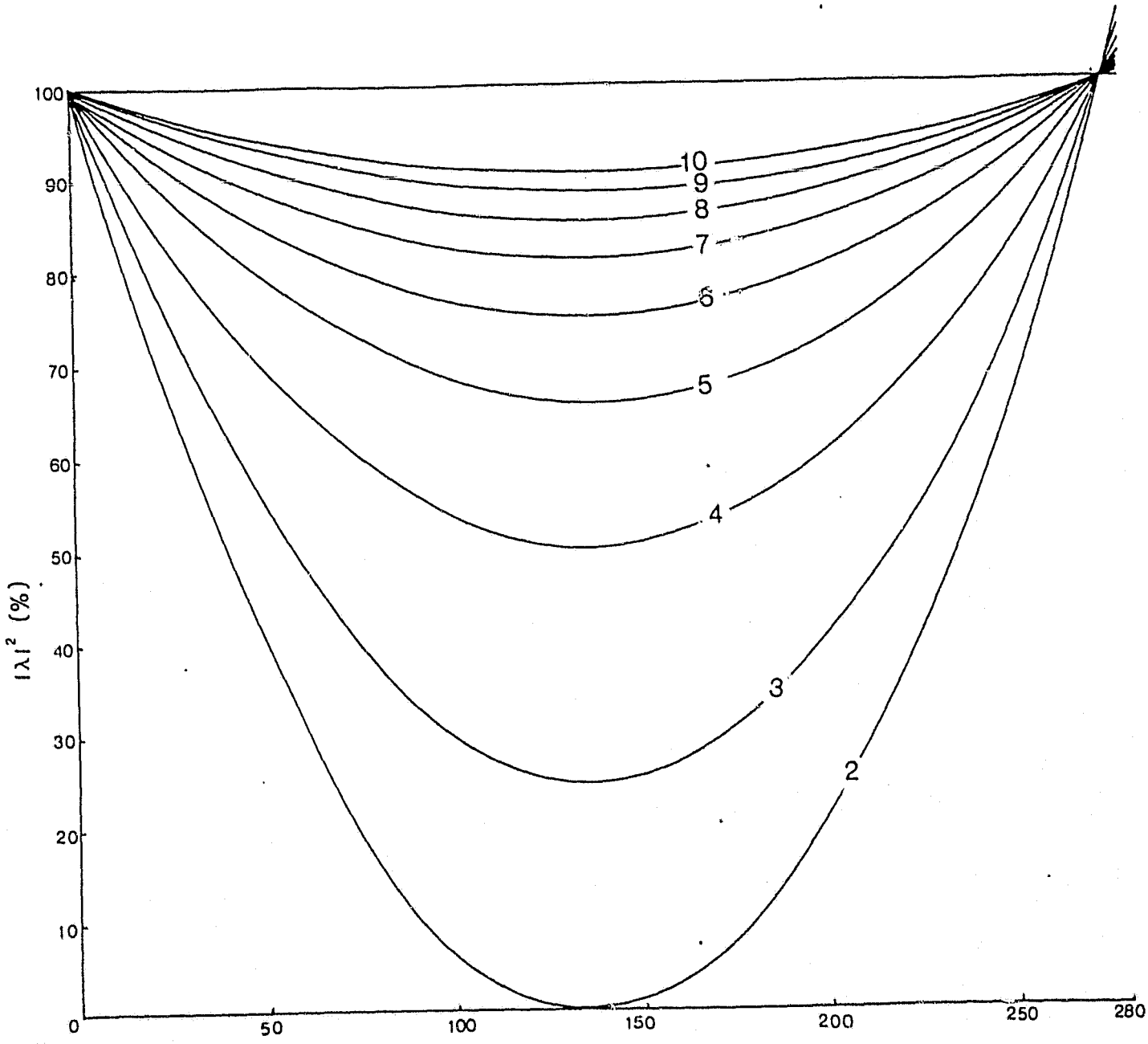

Fig. 4

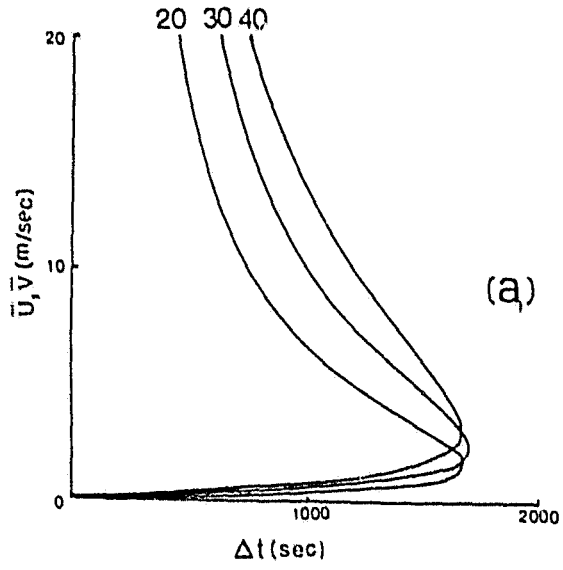

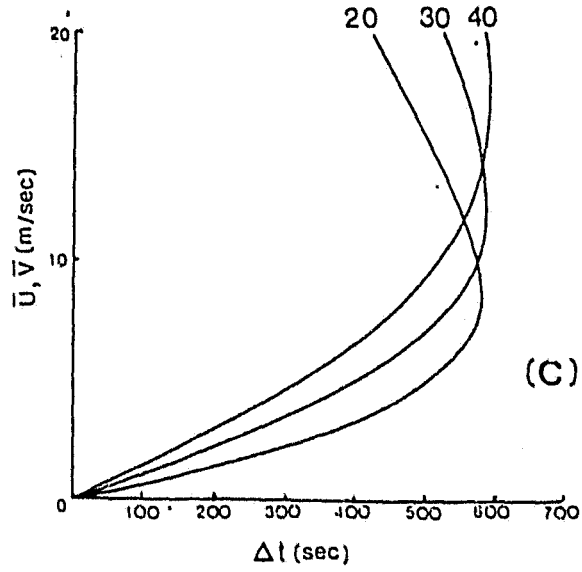

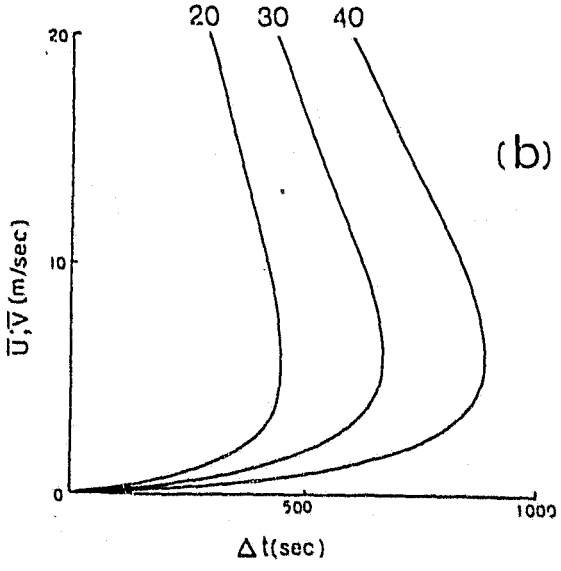

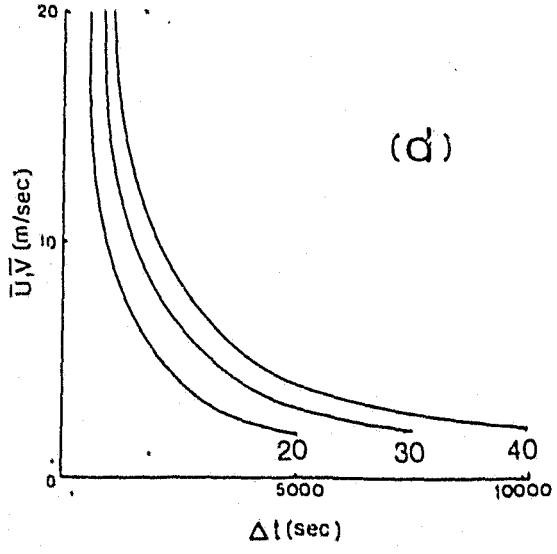

Fig. 5

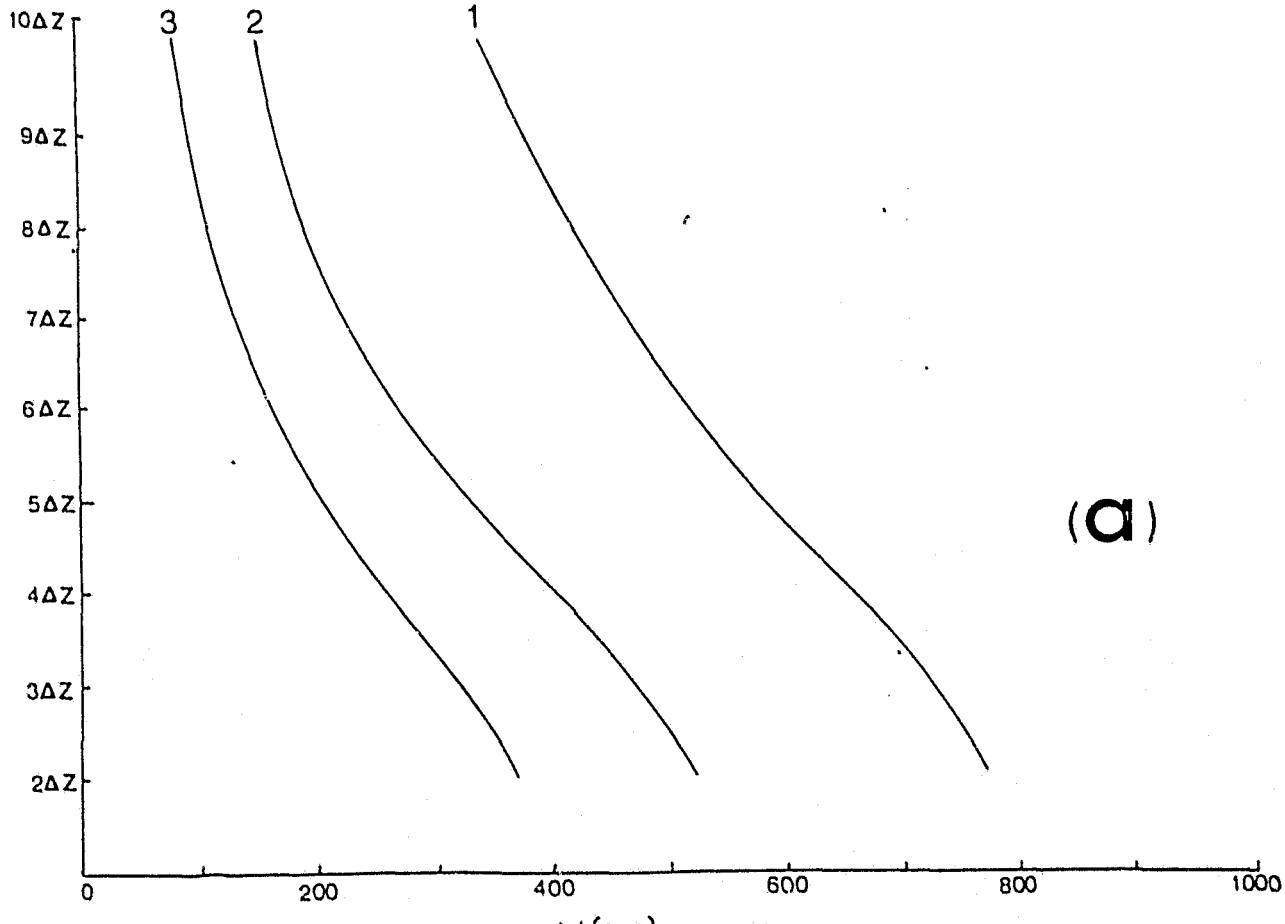

Fig. 5

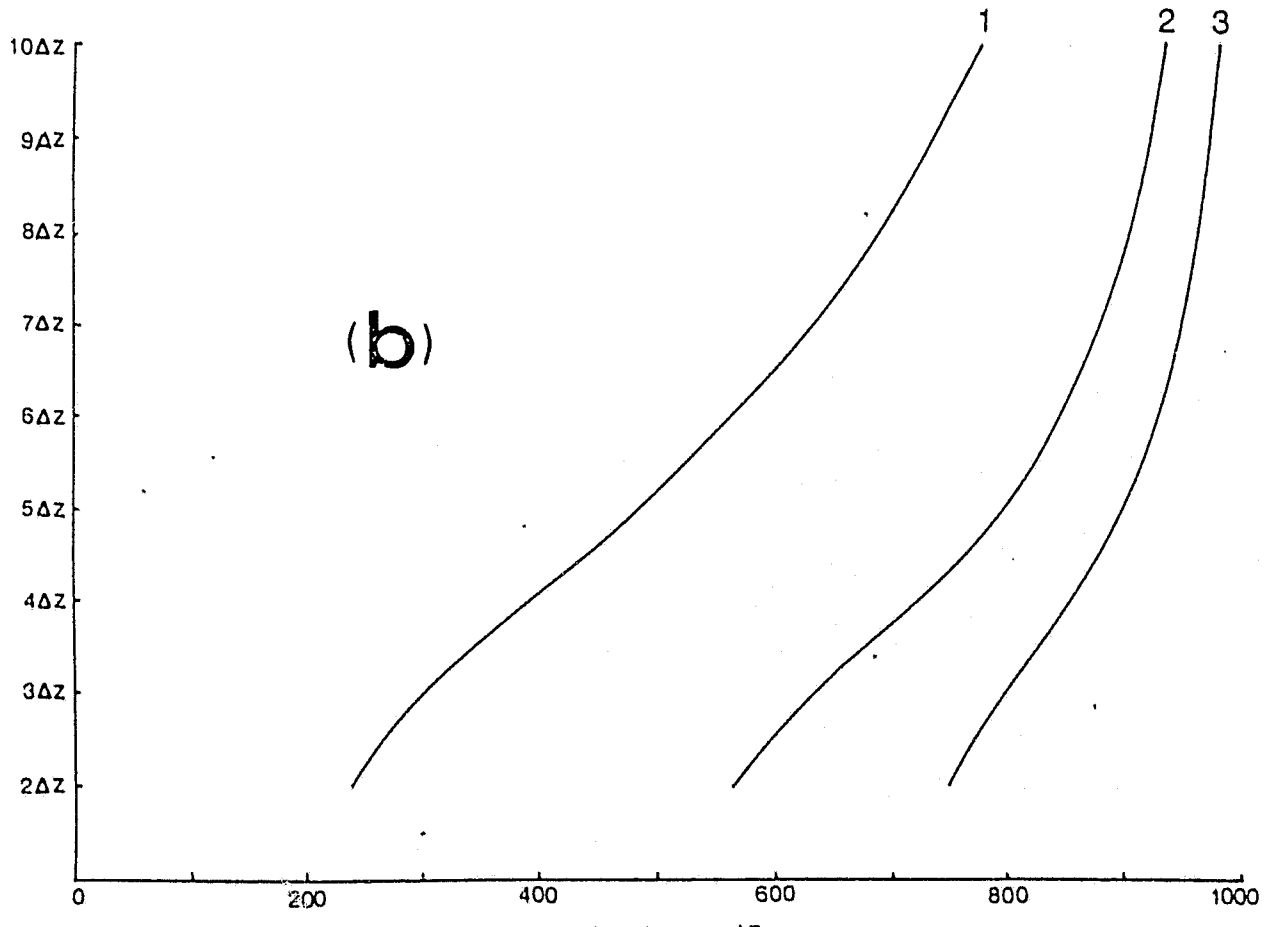

Fig 5

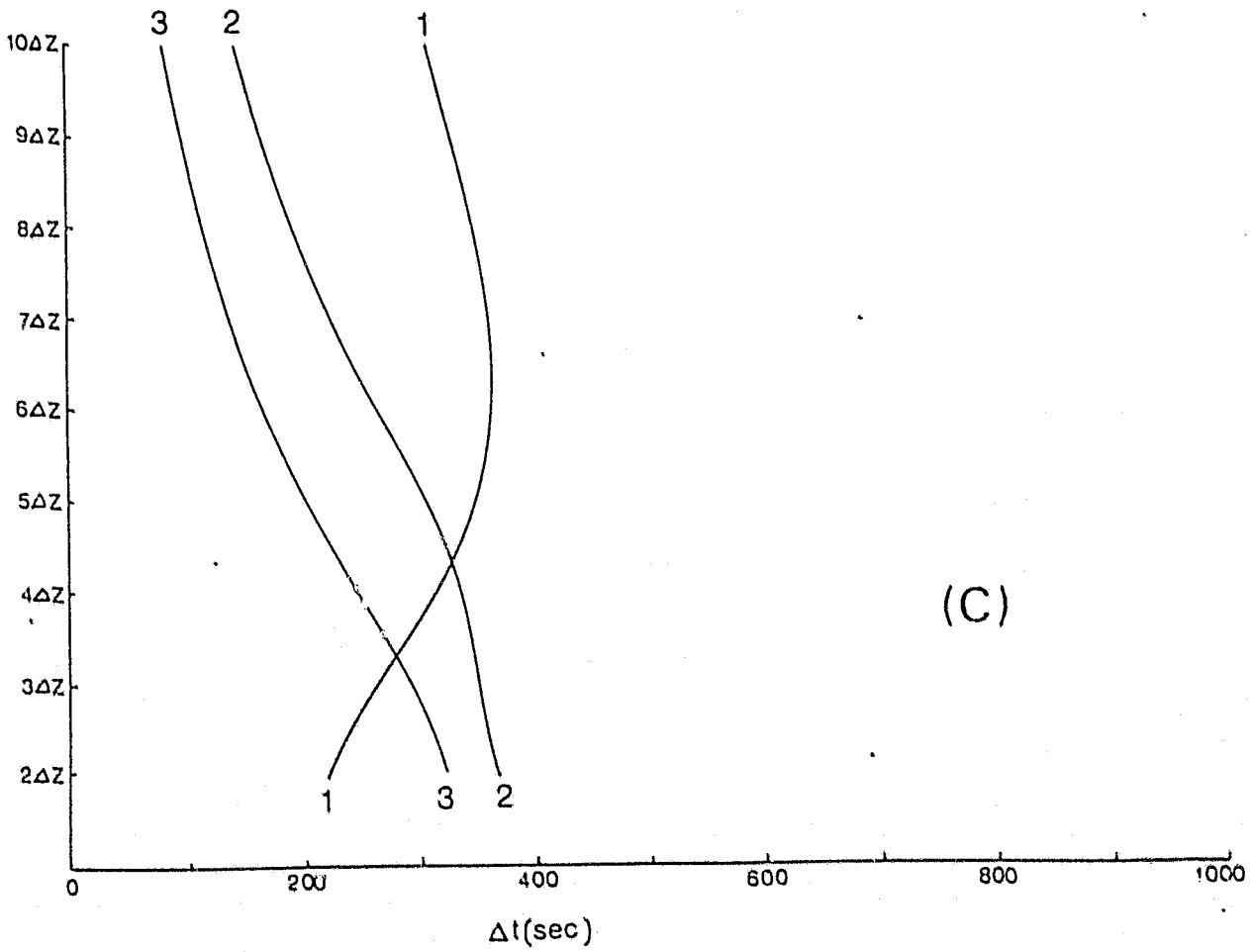

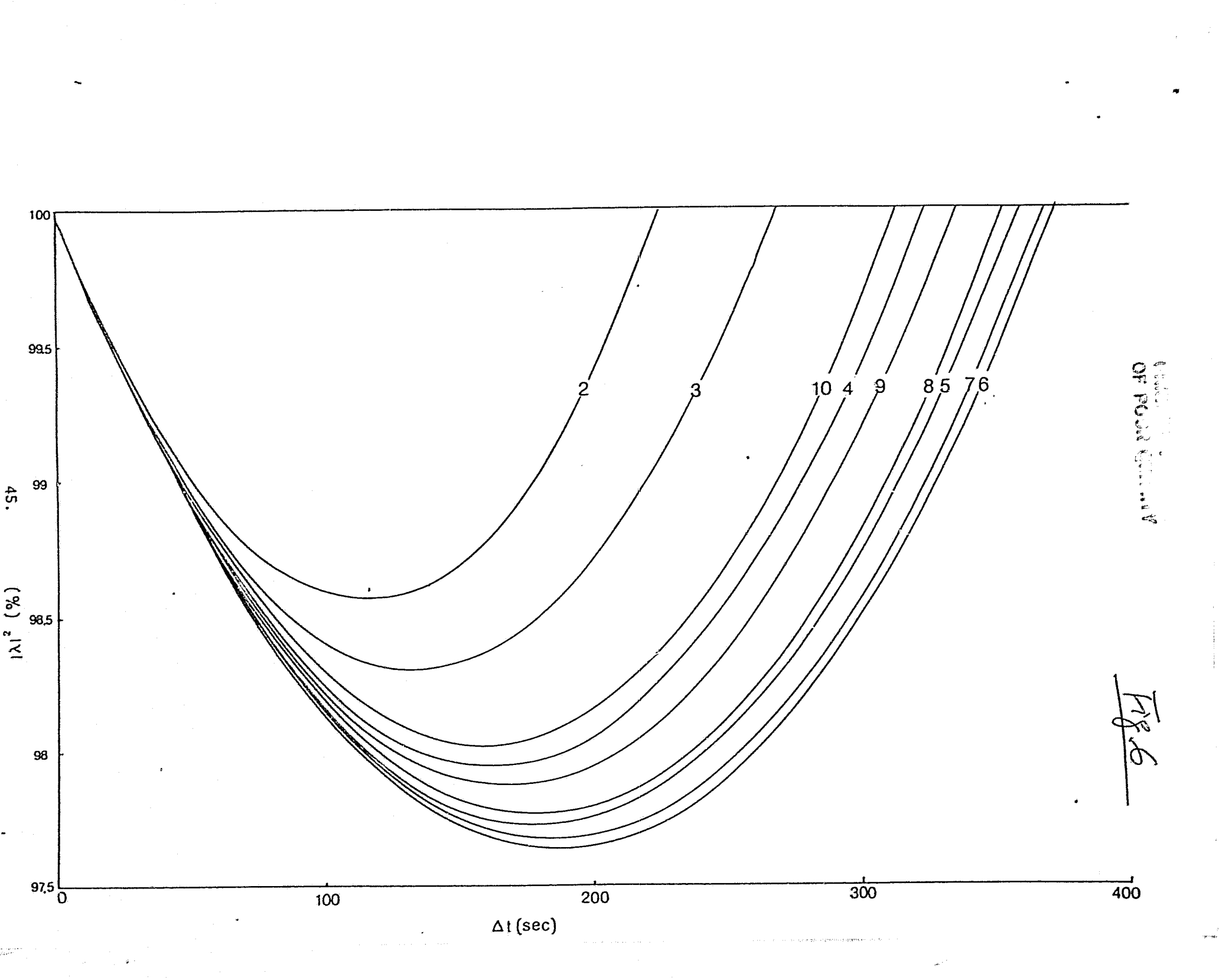
100
99.5
99
98.5
98
97.5
0
100
200
300
400
$|\lambda|^2$ (%)
Δt (sec)
2
3
10
4
9
8
5
7
6

References (Sec. II)

Byers, H. R., 1965. Elements of Cloud Physics, Chicago. The University of Chicago Press, 191 + ix pp.

Hamill, P., 1975. The time dependent growth of H_2O-H_2SO_4 aerosols by heteromolecular condensation. J. Aerosol Sci., 6. 475-482.

Hamill, P., C. S. Kiang, and R. D. Cadle, 1977. The nucleation of H_2SO_4-H_2O solution aerosol particles in the atmosphere. J. Atmos. Sci. 34, 150-162.

Hsu, H-m, 1979. Numerical simulations of mesoscale precipitation systems. Ph.D. Dissertation, Department of Atmospheric and Oceanic Science, The University of Michigan, Ann Arbor. 343 pp.

Kiang, C. S. and D. Stauffer, 1973. Chemical nucleation theory for various humidities and pollutants. Faraday Sym. 7, 26-33.

Reiss, H. J., 1950. The kinetics of phase transitions in binary systems. J. Chem. Phys. 18., 840-848.

IV. Acknowledgments

The prologue to our work under NASA Grant NSG-1243 is to be found in our prior research under the title "Rain Scavenging Studies" sponsored by AEC-ERDA-DOE under contract No. AT(11-1)-1407 during the years 1964-1978.

The present work has been done in close consultation with Dr. Gerald L. Pellett, NASA, Langley R.C. His interest in and comprehension of our work has been outstanding. He is, by far, the most informed, supportive and effective research liaison person with whom we have worked in 30 years of federally sponsored research under five different federal agencies.

Chapter 1 represents mainly work done by Mr. Brian G. Hicks, Ph.D. candidate.

Chapter 2 is the work of H-m Hsu, Ph.D., now Assistant Professor of Atmospheric Science, University of Wisconsin - Milwaukee.